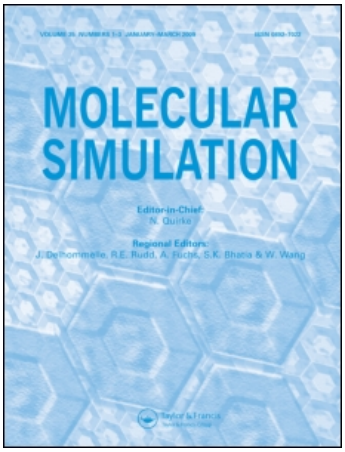

Molecular Simulation
Publication details, including instructions for authors and subscription information:
http://www.informaworld.com/smpp/title~content=t713644482

A molecular dynamics study of the effect of pentacene polymorphs on C_{60} surface adsorption and diffusional properties and the tendency to form nanowires

Rebecca Cantrell[a]; Paulette Clancy[a]
[a] Chemical and Biomolecular Engineering, Cornell University, Ithaca, NY, USA

Online publication date: 03 August 2010

To cite this Article Cantrell, Rebecca and Clancy, Paulette(2010) 'A molecular dynamics study of the effect of pentacene polymorphs on C_{60} surface adsorption and diffusional properties and the tendency to form nanowires', Molecular Simulation, 36: 7, 590 — 603
To link to this Article: DOI: 10.1080/08927022.2010.481795
URL: http://dx.doi.org/10.1080/08927022.2010.481795

Molecular Simulation
Vol. 36, Nos. 7–8, June–July 2010, 590–603

Taylor & Francis
Taylor & Francis Group

A molecular dynamics study of the effect of pentacene polymorphs on C_{60} surface adsorption and diffusional properties and the tendency to form nanowires

Rebecca Cantrell and Paulette Clancy*

Chemical and Biomolecular Engineering, Cornell University, 120 Olin Hall, Ithaca, NY 14850, USA

(*Received 9 January 2010; final version received 28 March 2010*)

Using atomic-scale molecular dynamics and energy minimisation techniques with semi-empirical molecular mechanics 3 potential energy functions, we consider the adsorption of a C_{60} molecule on pentacene in the known thin film and bulk phases and a series of hypothetical, variably angled, pentacene structures. The thin film phase has a more energetically isotropic surface than the bulk, and exhibits diffusion coefficients that are twice as high, potentially leading to preferable characteristics for ordered film growth. For the variably angled pentacene structures, where the long axis is parallel to the substrate, a relationship was discovered between the angle that the pentacene short axis makes with the surface normal (controlled by the underlying substrate) and the adsorption characteristics of C_{60}. There is a transition of the dominant energy minima from between the pentacene rows at low values of φ_1 to within the rows at high values of φ_1, where φ_1 is the angle the bottom pentacene short axis makes with the surface normal. This shift implies that the likelihood of forming C_{60} nanowires on pentacene is greater at extreme values of φ_1 for which there would be a clear preference for C_{60} to be located between a row or within a row, rather than at intermediate values of φ_1, where there is no clear preference.

Keywords: pentacene; molecular dynamics; C_{60} adsorption; C_{60} diffusion

1. Introduction

In recent years, considerable attention has been paid to the development of all-organic electronic devices, ranging from organic photovoltaic (OPV) devices and organic light-emitting diodes to organic thin film transistors (OTFTs). The drive for the development of organic semiconductor materials has been their potential to offer cheaper and larger-scale (roll-to-roll) processing than traditional inorganic semiconductors as well as the inherent flexibility that organic substrates offer. Although inorganic semiconductor materials generally have much higher charge carrier mobilities, recent progress has resulted in the development of p-type aromatic hydrocarbon materials, especially pentacene, which show comparable hole mobilities to those of amorphous silicon ($\geq 1\,cm^2/V\,s$) [1,2]. For organic n-type semiconductors, such as C_{60}, reported electron mobilities can be as high as $0.65\,cm^2/V\,s$ [3]. In this paper, we focus on studying the dissimilar interactions between p-type pentacene (abbreviated to Pn) and n-type C_{60} as an exemplar for a p–n heterojunction in an organic semiconductor system. This combination of materials has been studied experimentally for OTFTs [4,5] and especially for OPV devices [6,7], exploiting the absorbance properties of the system for use in photovoltaic devices.

Unlike many inorganic p–n junctions, organic p–n junctions carry charges by a localised hopping mechanism, which is generally assumed to be responsible for the lower charge carrier mobilities. Correspondingly, the diffusion length of an exciton (an electron–hole pair) in an OPV device is much lower, and hence the electron and hole only have a chance to split (the desired effect) if they are formed very near, or at, the p–n junction interface. Thus, knowing the atomic-scale details of the interface between the p- and n-type materials is very important for understanding the performance of organic semiconductor materials. An ideal heterojunction is assumed to be one in which both of the organic components forming the interface exist in as orderly and planar form as possible, which is often interpreted to mean highly crystalline. This order is desired in the bulk and at the interface so that there is very little charge scattering, which can otherwise lead to the undesirable result of electron–hole recombination. Despite this commonly acknowledged need to create a highly ordered interface, there has been very little experimental work to probe the nature of the C_{60}/Pn interface and even fewer computational studies.

It is possible to grow highly ordered pentacene films in the laboratory using a variety of techniques [8–10], but the ability to grow the desired ordered layers of C_{60} on top of pentacene in an ideal layer-by-layer manner is made more difficult by the tendency of C_{60} to cluster and dewet the pentacene surface and thus to grow in an undesirable three-dimensional fashion [11]. One key way to improve the growth behaviour of C_{60} on pentacene is to find a way to increase the mobility of the C_{60} molecules on the

*Corresponding author. Email: pqc1@cornell.edu

ISSN 0892-7022 print/ISSN 1029-0435 online

DOI: 10.1080/08927022.2010.481795
http://www.informaworld.com

pentacene surface in order to allow film-smoothening mechanisms to occur.

In this paper, we focus on C_{60} interactions with a variety of different pentacene surfaces that differ most strikingly in the angles that the short and long axes make with the surface normal. First, we compare two experimentally observed pentacene polymorphs, the so-called 'bulk' and 'thin film' phases, which differ slightly in the angle adopted by pentacene's *long axis* as it stands upright on the underlying *insulating* surfaces (see Figure 1). But on other substrates, primarily metals [12–15] and silicon [16,17], where opportunities to share electrons are more facile, pentacene lies down on the surface (i.e. its long axis is parallel to the surface) to an extent determined by the nature of the substrate. Thus, our second study considers a series of hypothetical situations in which we vary the angle that pentacene's *short axis* makes with the underlying substrate, keeping the long axis parallel to the surface (see Figure 2). This second study emulates situations found experimentally in which the tilt angle made by pentacene's short axis with the surface (shown as φ_1 in Figure 2) will be different depending on the metal upon which the pentacene is deposited. For instance, when two layers of pentacene are deposited on copper, there is a resulting angle of 65°–70° between pentacene's short axis and the surface normal [12]. In theory, the metal could be chosen to produce a desired short-axis tilt angle of the pentacene overlayers in order to control the adsorption behaviour of subsequent molecules.

For all pentacene phases studied here, real or hypothetical, we consider the mobility and anisotropy of the C_{60} molecules diffusing on the pentacene surface. The goal of this paper, then, is to shed some light on the trends of the adsorption and diffusion properties of the C_{60} molecules as we alter the corrugation of the pentacene surface via changing the angle that either pentacene's long axis makes with an insulating substrate (thin film vs. bulk phases) or that its short axis makes with the metallic substrates. In the latter case, since there are no 'phases' associated with these situations where pentacene's long axis lies flat but its short axis is tilted, we will address this issue by considering a range of short-axis tilt angles that are possible (from 10° to 90°) and suggest how to describe an analogue to the 'unit cell' of these situations. Our hypothesis is that the angles formed by pentacene molecules affect the ability of the 1 nm-diameter C_{60} molecules to fit into the 'hollows' of the surface created by the surface corrugation, which then affects surface diffusion and, potentially, structure-directing molecular processes (such as nanowire formation).

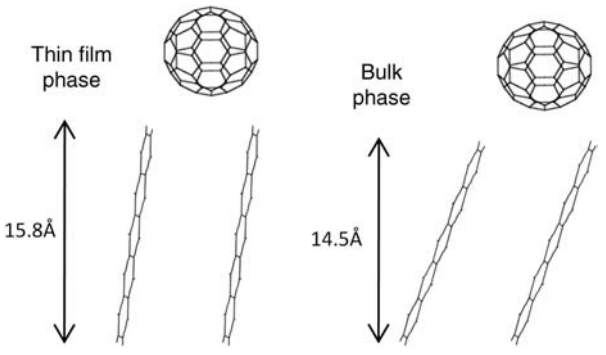

Figure 1. Side-view diagram illustrating the orientation and relative heights of the thin film and bulk phases of pentacene.

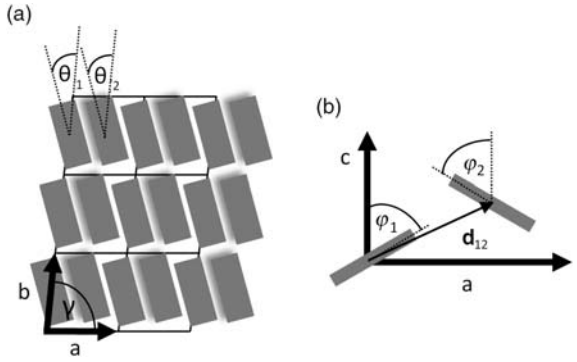

Figure 2. Schematic diagrams of the variably angled pentacene systems from (a) a plan and (b) a side view, illustrating the definitions of the parameters a, b, c, γ, θ_1, θ_2, φ_1, φ_2 and $\mathbf{d}_{12}$, which are listed in Table 1. Pentacene molecules are represented as grey rectangles for simplicity.

2. Background

2.1 Planar vs. bulk heterojunctions

Our studies emulate what is termed a 'planar heterojunction', rather than a 'bulk heterojunction'; the distinction being that the *bulk* heterojunction involves an interpenetrating blend of donor and acceptor molecules in an attempt to reduce the distance that an exciton has to travel to dissociate. The *planar* heterojunction, as its name implies, assumes a planar, non-interpenetrating interface. It has been found that bulk C_{60}/Pn heterojunctions have a slightly higher open-circuit voltage than planar heterojunction devices; however, their short-circuit current density and thus power conversion efficiency are approximately six times lower than those of planar C_{60}/Pn heterojunctions [18,19]. Not only do bulk heterojunctions tend to phase-separate and short-circuit, but there is also a large charge recombination rate due to the C_{60} molecules being positioned directly against the benzene-ringed 'face' of a Pn molecule, facilitating hopping [20]. This configuration occurs much less often in planar heterojunctions because C_{60} lies in the crevices between the Pn molecules, interacting with the end or edge of the molecule, not its 'face'. For these reasons, we focus solely on the planar C_{60}/Pn heterojunction.

2.2 Bulk and thin film phase pentacene

The bulk and the thin film phases appear when growing pentacene on electrically insulating substrates such as SiO_2 or Al_2O_3 using either low-pressure organic vapour phase deposition [21] or vacuum thermal evaporation [9]. As its name suggests, the thin film phase occurs during the first few monolayers of growth (at least). The ratio of bulk phase to thin film phase pentacene increases with deposition temperature, deposition pressure (for vapour phase deposition) and film thickness; other factors, such as deposition rate, affect the distribution of these polymorphs as well [9,22,23]. Thus, it is experimentally possible to control the polymorphism of the top pentacene layer to be either a thin film or a bulk phase [24]. The bulk phase has the well-accepted triclinic lattice parameters of $a = 7.90$ Å, $b = 6.06$ Å, $c = 16.01$ Å, $\alpha = 101.9°$, $\beta = 112.6°$ and $\gamma = 85.8°$, reported by Northrup et al. [25] based on X-ray diffraction results from Campbell et al. [26]. The thin film phase has the triclinic lattice parameters of $a = 7.56$ Å, $b = 5.93$ Å, $c = 15.65$ Å, $\alpha = 93.3°$, $\beta = 98.6°$ and $\gamma = 89.8°$, reported by Yoshida et al. [27] based on X-ray diffraction reciprocal space mapping.

Studies of C_{60}/Pn usually focus on the electronic properties (e.g. current–voltage curves and power conversion efficiencies) after the device formation [4–7]. However, there are a couple of previous studies which focus on the sub-monolayer growth of C_{60} on thin film pentacene. There is some inconsistency about whether C_{60} wets or dewets a thin film pentacene surface, the former outcome being much preferred. Itaka et al. [28] suggested that C_{60} wets a thin film layer of pentacene on Al_2O_3, whereas Conrad et al. [11] showed that C_{60} on a thin film layer of pentacene on SiO_2 does not wet the surface. Itaka et al. grew 20 nm-thick C_{60} films on Al_2O_3 and found that C_{60} formed crystalline grains as large as 600 nm with very smooth surfaces. Conrad et al. grew up to 0.25 ml of C_{60} on 1.6 ml of thin film pentacene on SiO_2 and found that C_{60} forms small three-dimensional 'roughly spherical' clusters several nanometres tall. Thus, the Conrad et al. paper shows C_{60} dewetting the surface. Superficially, these contradictory observations could be ascribed to the difference in substrates used by the two groups, but this seems unlikely since the dielectric surfaces in each case are at least 20 Å away from the centre of the C_{60} molecules (i.e. out of the range of influence even without a screening pentacene layer). A more likely cause is that Itaka et al. used a deposition rate twice as slow as that of Conrad et al. If the deposition rate is very high, the C_{60} molecules may not have as much chance to diffuse before they encounter another deposited molecule, thus causing a higher density of smaller islands. In order to theorise further about the growth mode of C_{60} on pentacene, by classical nucleation theory, for example, the details of the C_{60}/Pn kinetics (e.g. energy barriers and diffusion coefficients) need to be known, and the results in this paper will facilitate such a study.

Previous molecular dynamics (MD) simulations have shown that, at room temperature, the diffusion coefficient of C_{60} on bulk phase pentacene is 5.8×10^{-5} cm^2/s [29], but the thin film pentacene phase was not considered. In Section 4.1, we compare and contrast the diffusion behaviour of C_{60} on both bulk and thin film phase pentacene. We will show that diffusion coefficients, in combination with adsorption energy surface maps, provide insight into which polymorphs might yield better growth properties of C_{60} on pentacene.

2.3 Motivation to vary the short axis of pentacene adsorbed on metallic substrates

In contrast to the bulk and thin film structures adopted by pentacene on most insulating surfaces, such as thermal oxides, the first monolayer or so of the pentacene molecules is known to lie essentially flat on some substrates, typically metals [12–15], but also silicon [16,17]. This 'flat' pentacene structure can only occur for the first few monolayers depending on the balance of the strength of the Pn–Pn interactions vs. the Pn–metal interactions; for thicker Pn films, subsequent pentacene monolayers orient themselves nearly upright in the thermodynamically stable herringbone structure to maximise the overlap of their π-orbitals [12,15]. Dougherty et al. [30] deposited C_{60} on two layers of pentacene on Ag(111) and found that, at low C_{60} coverage, C_{60} nanowires form between the pentacene rows. This phenomenon is exciting because it suggests that when pentacene is angled close to the underlying surface, it might serve as a 'templating' material for more ordered, and directionally biased, growth of C_{60}. Dougherty et al. found the first monolayer of pentacene on Ag(111) to lie flat on the substrate, but, in the second layer of pentacene, the molecules' short axis is oriented approximately 28°–34° off the surface (i.e. a surface normal angle, φ_1, of 62°–56° in the convention we adopt, described in Section 4.4 and Appendix). Since C_{60} nanowire formation on pentacene has not been observed elsewhere in the literature, this specific pentacene orientation on Ag(111) found by Dougherty et al. could be just right to allow the formation of C_{60} nanowires in the crevices between the pentacene rows. Investigating whether there is indeed a 'sweet spot' for the angle of the Pn molecules to hold or orient the C_{60} molecules provided additional motivation for us to study, in Section 4.4, the energetic minima for C_{60} molecules on pentacene as we vary the angle of the short axis of pentacene over a range of possible angles (from 10° to 90°).

3. Methods

3.1 MD simulations

As described in a previous paper [29], all simulations performed and reported here were carried out using the

freeware software package TINKER, which is an atomic-scale (all-atom) modelling package using MD techniques for a choice of semi-empirical potentials [31]. Within the MD simulations, the Beeman integration method was used to obtain positions, velocities, accelerations and relevant system energies at each integration step (a time step of 0.5 fs). For each simulation, a short thermalisation run of 5 ps was performed using a canonical ensemble in which a specified equilibrium temperature is achieved and maintained using a Berendsen thermostat [31]. Once the system reached the desired temperature without significant fluctuations ($\pm < 3$ K), the simulation was continued using a microcanonical ensemble (which maintains constant energy) for a further 2 ns. In order to improve the statistics of the results, simulations of all the systems reported here were repeated 10 times each. The fluctuating average local pressure in the system was 10 ± 210 atm, exhibiting the typical large pressure fluctuations seen in NVE simulations. Each system of 10 runs was carried out for temperatures between 200 and 600 K, designed to include a range of temperatures similar to that used in experimental studies of C_{60} on the surface of pentacene [32].

For MD simulations of a single C_{60} molecule on both thin film and bulk phases, the computational system consisted of two Pn layers with the bottom layer fixed and the top layer free to move. Each layer involved a reasonably large system size of 5×5 pentacene unit cells (50 molecules) to limit spurious system-size effects. For simulations of C_{60} on bulk and thin film pentacene, the coordinates of the centre of mass of the adsorbed molecule were tracked to allow us to calculate surface diffusion coefficients, to perform an energy barrier analysis and to undertake an adsorption energy surface mapping of the C_{60}/Pn systems using a combination of MD and static total-energy calculations. For the subsequent MD simulations of 48 pentacene molecules lying at varying angles on Si, as discussed in Appendix, a Si(001) surface consisting of three atomic layers was fixed, while the pentacene molecules lying on top of them were free to move. Periodic boundary conditions were applied here as well to allow the pentacene cluster to move freely. This simulation was thermalised at 300 K in the NVT ensemble for 50 ps and then run in the NVE ensemble for a further 2 ns.

The most important input for an MD simulation is the choice of intermolecular potential model. The molecular mechanics 3 (MM3) potential model used in this paper is the same as that reported in a previous paper [29]. We chose this semi-empirical MM3 force field since it has been shown by its developers to accurately describe hydrocarbons, namely three-, four-, five- and six-ringed structures [33]. MM3 incorporates stretching, bending and torsional energies as well as the van der Waals interaction energies based on atom–atom parameters related to their chemical environment [33]. Prior to our simulations, we confirmed that the MM3 model was suitable for the two molecules in our system. For pentacene, we had already confirmed that the MM3 potential accurately reproduced *ab initio*-derived MP2 intermolecular energies and predicted the correct lowest energy herringbone structure as a prelude to extensive studies that showed that the MM3 model reproduces experimental sticking coefficients and other experimentally observed phenomena [34]. For the C_{60} intermolecular potential, we verified that the MM3 potential was similar to *ab initio* calculations of the C_{60}–C_{60} interactions produced by Pacheco and Prates Ramalho [35], which were carried out in the local density approximation to density functional theory (DFT), together with its extension for excited-state time-dependent DFT. Thus, we are confident that the semi-empirical MM3 potential was sufficiently accurate to model the C_{60} interaction with pentacene polymorphs.

3.2 Adsorption energy surfaces

For pentacene in all the forms we studied (bulk and thin film phases, and for cases where we varied the Pn short axis angle with respect to the surface normal), we calculated the potential energy surfaces that would arise from the adsorption of a C_{60} molecule. These energy surfaces provide insight into the manner in which a C_{60} molecule probes the different pentacene surfaces and any tendency to favour lower energy sites. The potential energies were calculated statically using the TINKER software with the MM3 potential. Each energy value shown in the contour plots (Figure 4, for instance) represents the energy between one C_{60} molecule and the pentacene surface, so as to roughly represent absorption energy at different points along the surface. The increments in the x- and y-directions by which the C_{60} scanned the surface were chosen such that there was no increment step greater than 0.4 Å for a given system. Although C_{60} is approximately spherical, it has faceted edges which slightly influence the adsorption energy. Thus, for each point along the surface, the adsorption energy was calculated by averaging over 10 random orientations of the C_{60} molecule to smooth out any contributions from the non-sphericity. We also considered the height of the C_{60} above the surface at different points along the surface. For each set of x–y points, we determined the height above the surface that gave the minimum energy (chosen to within 0.1 Å in the z-direction). This was the method used to obtain the adsorption energy surfaces of C_{60} on the bulk phase, thin film phase and variably angled pentacene systems.

For the thin film and bulk phase adsorption energy calculations, the structures of these pentacene substrates were given by their known triclinic unit cell lattice parameters [25,27]. For the variably angled pentacene, however, there is no commonly accepted crystalline structure because its structure is influenced by the

Table 1. Summary of unit cell parameters considered in the formation of the hypothetical, variably angled, pentacene structures[a].

Parameter	Value	Obtained from/by	Fixed in geometry optimisation?
a	5 Å (initial guess)	Recursive minimisation	Yes
b	15.6 Å	MD snapshot	Yes
c	N/A	N/A	N/A
α	N/A	N/A	N/A
β	N/A	N/A	N/A
γ	86.5°, 76.5°	MD snapshot	Yes
θ_1, θ_2	10.1°	MD snapshot	θ_1 Yes, θ_2 No
φ_1, φ_2	10°–90°	Independent variable	φ_1 Yes, φ_2 No
$\mathbf{d}_{12}$	$\langle a/2, b, 5$ Å$\rangle$ (initial guess)	Guess	No

[a]Described in detail in Appendix.

substrate underneath. For these adsorption energy surfaces, we performed a parameter sensitivity analysis, varying some parameters and estimating others to determine the adsorption energy surfaces as a function of the angle made by the pentacene with the underlying substrate. The exact procedure we used for this is given in Appendix. Figure 2(a) and (b) gives schematics of the variably angled pentacene molecules to show the parameters involved, and Table 1 provides their values. Angles φ_1 and φ_2 are those that the short axes of the bottom and top pentacene molecules make with the surface normal clockwise and anticlockwise, respectively. With φ_1 being the independent variable, $\varphi_1 = 10°$ corresponds to the short axis of pentacene standing nearly upright, and $\varphi_1 = 90°$ corresponds to the pentacene lying on its face, flat on the surface.

The angle γ is the angle between lattice vectors **a** and **b**, as shown in Figure 2(a). Values for γ were obtained by different MD snapshots, and they ranged from about 60° to 110°, with an average of 86.5°. The spread of these values is not symmetric (see Figure A2), with the most probable value for γ being less than the average. To determine the sensitivity of our results to the choices made for angles such as γ, we chose an additional angle to test, $\gamma = 76.5°$, because it is within the range of most probable values and is, conveniently, exactly 10° less in value. More details about the choice of γ are given in Appendix. In summary, for the adsorption energy surfaces for variably angled pentacene, we studied two cases of $\gamma = 76.5°$ and 86.5°, and for each, we vary φ_1 from 10° to 90° in increments of 10°.

4. Results and discussions

4.1 MD trajectories: thin film vs. bulk

Comparing the nature of the C_{60} diffusion behaviour on the two experimentally observed pentacene phases (thin film and bulk), we found interestingly different behaviour. Figure 3(a) and (b) shows plan views of their MD-determined trajectories at 300 K for each phase. Each point on the graphs represents the C_{60} centre-of-mass point location at 1 ps intervals for a total of 2000 points, or 2 ns. The most obvious difference between these two trajectory images is that there appears to be a strong anisotropic diffusion component for the C_{60} diffusion on bulk-phase pentacene (Figure 3(b)), manifesting itself as a tendency to move in preferred directions over the surface. This is not found on the thin film phase pentacene, Figure 3(a), which resembles a typical random walk over the surface. This anisotropy on bulk phase pentacene was discussed in our

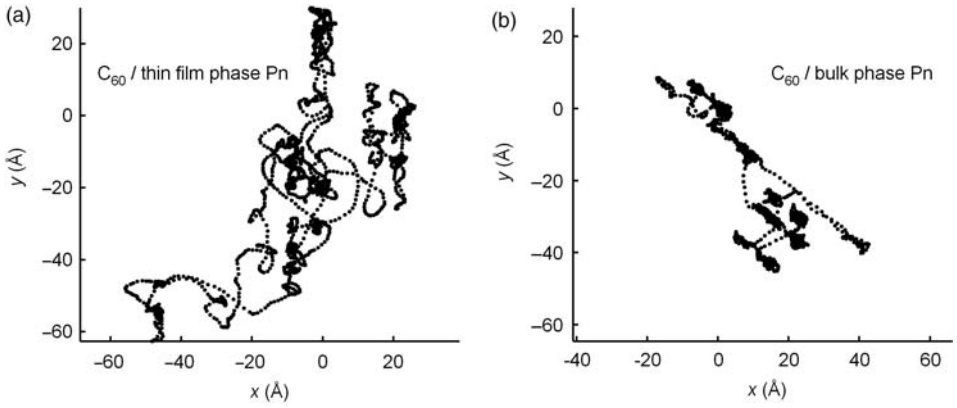

Figure 3. MD-generated x–y trajectories of the centre of mass of one C_{60} molecule on (a) thin film phase pentacene and (b) bulk phase pentacene. The black dots represent the location of the molecule at 1 ps increments, for a total of 2 ns each.

previous publication [29], but here it is described in further detail and contrasted to the diffusion of C_{60} on the thin film Pn phase. Since the only difference between these two systems is the pentacene phase, there is something implicit about the nature of the bulk phase Pn that causes the C_{60} molecule to diffuse anisotropically. To explore this difference, we first consider the physical characteristics of the systems. Based on the unit cell parameters of the bulk and thin film phases of pentacene, the differing angle of the film with the underlying surface gives rise to a vertical distance of a thin film phase layer of 15.8 Å, while that of the bulk phase is only 14.5 Å, as shown in Figure 1. In terms of molecules per unit area of the Pn(001) surface, the surface density of the thin film phase is 7% higher than that for the bulk phase. A higher surface density suggests a less corrugated surface with less prominent places for the C_{60} molecules to get trapped. This suggestion is borne out by the diffusion behaviour (Figure 3(b)) where there are more locations of extended occupation in the bulk phase than in the thin film (Figure 3(a)), suggesting that the former has corrugations that hinder diffusion.

4.2 *Adsorption energy surfaces: thin film vs. bulk*

To further explore the origin of the hindered diffusion for the bulk phase compared to the thin film phase, we look at the details of the pentacene surface experienced by a C_{60} molecule through adsorption energy surfaces of C_{60} on thin film (Figure 4(a)) and bulk phases (Figure 4(b)). It is clear from these contour energy plots that the bulk phase (Figure 4(b)) pentacene has deeper energy wells (and higher energy peaks) that a C_{60} molecule can access in comparison to the thin film phase. This is supported by the evidence of trapping shown in the MD trajectories in Figure 3(b). In addition, the anisotropy of the adsorption energy surface is manifest in the diagonal low-energy 'valleys' (shown in aqua) and the differences between two types of energy peaks that form between the pentacene molecules. These diagonal valleys correspond to the anisotropic 'runs' of C_{60} shown in Figure 3(b). In contrast, the adsorption energy surface of the thin film phase in Figure 4(a) is relatively symmetric, with no clearly preferred direction for a C_{60} molecule to traverse and with a set of roughly equivalent and less steep energy peaks.

4.3 *Diffusion coefficients: thin film vs. bulk*

Using the MD trajectory data described in Section 4.1, we analysed the two-dimensional surface diffusion behaviour of C_{60} on both thin film and bulk phase pentacene, in addition to looking at the one-dimensional anisotropic diffusion behaviour in the $[1\,\bar{1}\,0]$ direction of the Pn(001) surface. For two-dimensional diffusion, the surface diffusion coefficient, D, was obtained using the Einstein equation, $\langle r^2 \rangle = 2dDt$, where $\langle r^2 \rangle$ is the observed mean-squared displacement of the diffusing admolecule, d is the dimension of the range of significant movement (two in the case of surface diffusion) and t is the time. The mean-squared displacement was measured as an ensemble average over many time intervals; we used 141 time origins at 100 ps intervals. Einstein's equation is based on the assumption that Brownian motion is present in the case where $\langle r^2 \rangle \sim t^n$, with $n = 1$. If $n > 1$, the process is said to be superdiffusive and, if $0 < n < 1$, the process is termed as subdiffusive [36]. In order to confirm which type of diffusional classification represents the motion of C_{60} on pentacene, we determine this power-law coefficient, n, from a log–log plot of the mean-squared displacement vs. time. Figure 5 shows the power-law coefficient, n, obtained at different temperatures for both the bulk phase and thin film phases. For both phases at all temperatures, the values for n have error bars that encompass the $n = 1$ value, thus the behaviour of the C_{60} on either phase of pentacene is indeed pure diffusion.

Regarding the Einstein equation, the values of the surface diffusion coefficients were found by plotting $\langle r^2 \rangle$ as a function of time, t, and dividing the resulting slope by 4 at long times. Figure 6 shows the surface diffusion

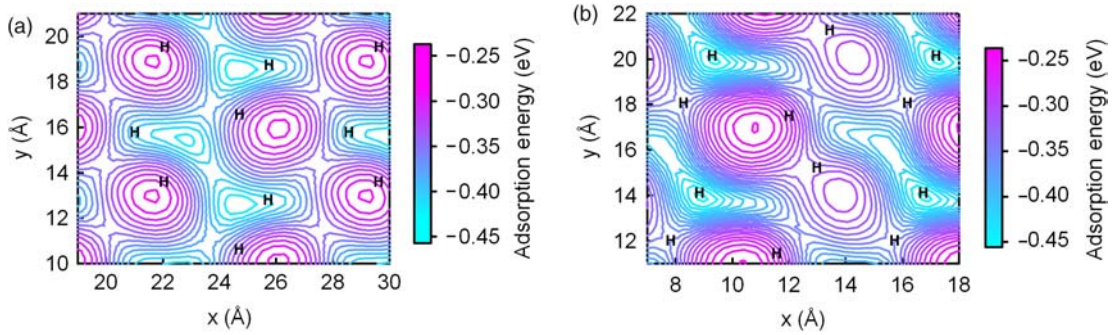

Figure 4. Adsorption energy maps of C_{60} on (a) thin film and (b) bulk phases of pentacene. The H letters indicate the location of the top hydrogen positions of the pentacene molecules with which the C_{60} molecules are in contact. Magenta colours signify high-energy areas; aqua colours signify low-energy areas (colour online).

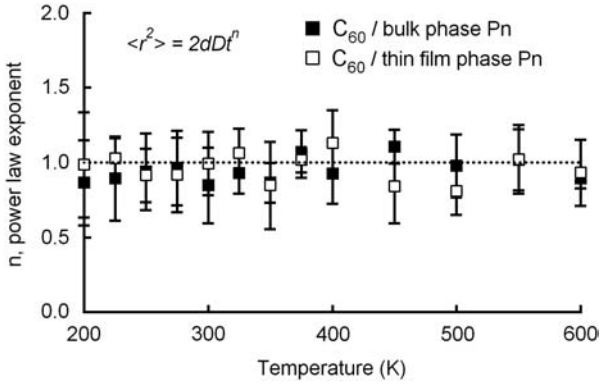

Figure 5. Power-law exponent, n, obtained from mean-squared displacement vs. time ($\langle r^2 \rangle$ vs. t) data from MD simulations, as a function of temperature. The exponent n is calculated from $\langle r^2 \rangle = 2dDt^n$, where $n = 1$ yields the Einstein equation and implies typical Brownian motion behaviour. In all cases, the MD-derived power-law exponent is close to 1.

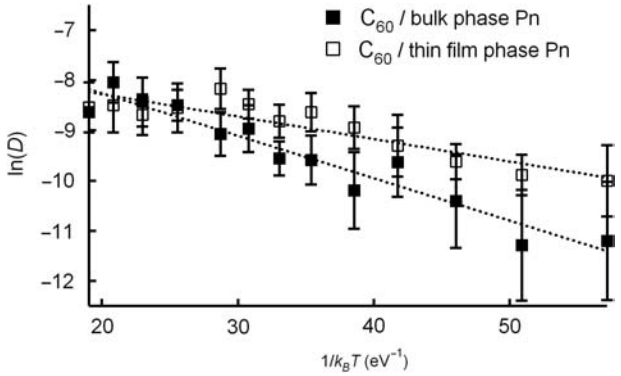

Figure 7. The natural logarithm of the surface diffusion coefficient vs. the inverse of k_BT, where k_B is the Boltzmann constant and T is the temperature. The dotted lines guide the eye to the linearity of the data. Following Arrhenius's theory, the steeper slope of the filled square data (bulk phase Pn) corresponds to a larger energy barrier than the open square data (thin film phase Pn).

coefficients of C_{60} on thin film and bulk phase pentacene. At and above a temperature of 500 K, the C_{60} molecule actually desorbed from the surface during some of the MD simulation runs, and the diffusion coefficients for those cases were not included in the averages quoted. With fewer diffusion coefficients in these cases, the average values for temperatures greater than 500 K have less statistical significance, signified by the grey background in Figure 6. Disregarding these higher temperatures, the surface diffusion coefficients of C_{60} on thin film phase were, for the most part, higher by about a factor of 2. This is consistent with the picture painted in Sections 4.1 and 4.2 for the ability of C_{60} to become trapped in low-energy wells on the *bulk* pentacene surface, but not on the *thin film* phase of pentacene, as evidenced by Figures 3 and 4.

Considering the temperature dependence of the observed diffusion, shown in Figures 6 and 7, where the data from Figure 6 are replotted as $\ln(D)$ vs. $1/k_BT$, the behaviour of C_{60} on pentacene can be assumed to be roughly Arrhenian. Assuming a linear fit to the data in Figure 7, values for the prefactor (D_0) and activation energy (E_a) in the Arrhenius equation, $D = D_0 \exp(E_a/k_BT)$, were found to be $D_0 \sim 1.4 \times 10^{-3}\,\mathrm{cm^2/s}$ and $E_a \sim 0.084\,\mathrm{eV}$ for the bulk phase and $D_0 \sim 6.2 \times 10^{-4}\,\mathrm{cm^2/s}$ and $E_a \sim 0.045\,\mathrm{eV}$ for the thin film phase. The energy barrier that the C_{60} needs to overcome in order to diffuse on bulk phase pentacene is almost twice as high as that on thin film pentacene, which corresponds well with the energy barrier values indicated from the adsorption energy surfaces in Figure 4.

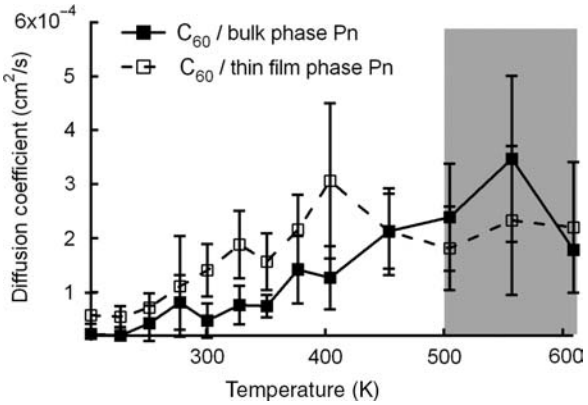

Figure 6. Surface diffusion coefficients of C_{60} on bulk phase Pn (filled squares) and thin film phase Pn (open squares) as a function of temperature. The grey region signifies a lack of statistically significant data due to desorption of C_{60} molecules from the pentacene substrate.

While the anisotropic behaviour of C_{60} on the bulk phase pentacene, as shown in Figure 3(b), is *qualitatively* apparent by eye, in order to *quantitatively* describe the diffusion of the C_{60} in one dimension, we map the vector displacements onto a particular direction. Here, we compare the diffusion of C_{60} in the $[1\,\bar{1}\,0]$ direction to that of the orthogonal [1 1 0] direction for both the thin film and bulk pentacene surfaces. We utilise the Green–Kubo relation for diffusion given by:

$$D = \frac{1}{d}\int_0^\infty \langle \mathbf{v}(0)\cdot\mathbf{v}(\tau)\rangle \,\mathrm{d}\tau \qquad (1)$$

and the corresponding velocity autocorrelation function,

$$C_{vv}(\tau) = \langle \mathbf{v}(0)\cdot\mathbf{v}(\tau)\rangle. \qquad (2)$$

Formally, the Green–Kubo relation is equivalent to the Einstein relation in the sense that it relates the macroscopic phenomenon of diffusion to microscopic transport phenomena. However, we use the Green–Kubo method

here with velocity autocorrelation functions to provide a measure of direction relative to the velocity at non-equilibrium time spans. As for the ensemble average, normally this involves an average of values of a large number of particles; however, in this case, we have one particle, so the ensemble average becomes an average over values at different time origins, as shown in the equation

$$\langle \mathbf{v}(0)\cdot\mathbf{v}(\tau)\rangle = \frac{1}{N_{\text{origins}}}\sum_{k=1}^{N_{\text{origins}}} \mathbf{v}(t_k)\cdot\mathbf{v}(t_k+\tau), \qquad (3)$$

where $N_{\text{origins}} = N_{\text{steps}} - \tau + 1$.

To obtain the directional diffusion coefficients, $D_{1\bar{1}0}$ and D_{110}, the Green–Kubo equations become:

$$D_{1\bar{1}0} = \frac{1}{d}\int_0^\infty \langle \mathbf{v}_{1\bar{1}0}(0)\cdot\mathbf{v}_{1\bar{1}0}(\tau)\rangle \,\mathrm{d}\tau, \qquad (4)$$

$$D_{110} = \frac{1}{d}\int_0^\infty \langle \mathbf{v}_{110}(0)\cdot\mathbf{v}_{110}(\tau)\rangle \,\mathrm{d}\tau, \qquad (5)$$

where the integrations of the autocorrelation functions were performed numerically.

Figure 8 shows these one-dimensional diffusion coefficients as a function of temperature for both the thin film and bulk phase pentacene. For the thin film phase, there is no significant difference between diffusion of C_{60} in the [1 $\bar{1}$ 0] and [1 1 0] directions, as further evidenced by the lack of anisotropy shown in Figures 3(a) and 4(a). However, for the bulk phase, diffusion in the [1 $\bar{1}$ 0] direction is consistently higher than that in the [1 1 0] direction, which provides a quantitative assessment of the anisotropy in the diffusion phenomena for this bulk phase polymorph.

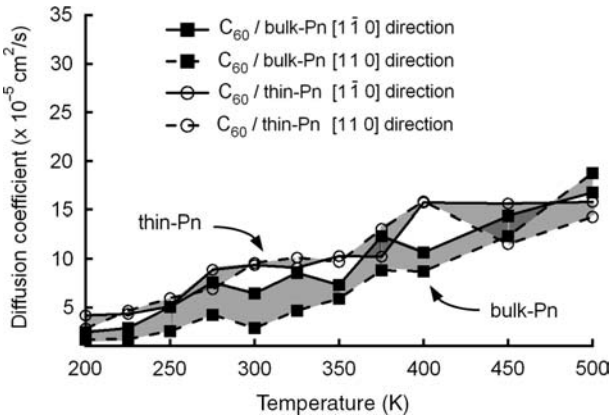

Figure 8. One-dimensional diffusion coefficients of C_{60} on Pn in the [1 $\bar{1}$ 0] direction (solid lines) and the [1 1 0] direction (dashed lines). There is a directional bias for diffusion on the bulk phase substrate (filled squares), but not for the thin film phase substrate (open circles). Consistent with Figure 6, C_{60} diffusion coefficients for bulk phase Pn have consistently lower values than for the thin film phase.

4.4 Variably angled pentacene

For the situations in which we allow the angle between the short axis of the pentacene molecules and the surface to vary (from 10° to 90°), we did not consider the dynamic properties of C_{60} on this pentacene surface because it was unknown to us how to accurately tune the intermolecular forces of the substrate beneath the pentacene such that the system would (spontaneously) give rise to the various angles we wished to study. Fixing the pentacene layer beneath the top flat layer of pentacene would have been an option, but since this bottom layer of pentacene is within the range of the C_{60} potential, making that lower layer rigid would have been unrealistic for dynamic simulations and could have led to unpredictable consequences. Thus, for the variably angled pentacene studies, we considered only the potential energy surface, which (as we have reported in Sections 4.1 and 4.2 for bulk and thin film pentacene) is likely to mirror the results obtained from MD simulations. Accordingly, we calculated the static adsorption energy surface of C_{60} on pentacene at various short-axis angles to the surface as shown in Figure 9 and used that as the metric for the behaviour of these situations.

Since the pentacene film in Dougherty et al.'s work is the only one in the literature that has observed nanowire formation of C_{60} on pentacene, we chose this as our test system. As described in Section 3.2 and Appendix, we emulated Dougherty et al.'s flat-lying pentacene system by also using two layers of pentacene and varying the short-axis angle φ_1 that controlled the pentacene film's degree of 'flatness' on the surface. We then observed the effect this had on the adsorption energy surface. We considered how the value of φ_1 affects both the *depth* of the energy wells, i.e. to provide sites of likelier adsorption, and the *width* of the energy wells to see their ability to accommodate the C_{60} molecule in a suitably sized 'pocket' on the surface.

The contour plots in Figure 9 show adsorption energy surfaces for $\gamma = 76.5°$ as we vary φ_1 (shown for 10°, 50° and 90°). The angle γ is the angle between lattice vectors **a** and **b**, as shown in Figure 2(a), and the $\gamma = 76.5°$ choice is discussed in Section 3.2 and Appendix. Although more data for the contour energy plots were taken at intermediate values of φ_1, this set of contour plots in Figure 9 shows the general trend. The contour plots for $\gamma = 86.5°$ (left out in Figure 9) looked qualitatively very similar to those of $\gamma = 76.5°$, implying that the adsorption energy patterns are not overly sensitive to the choice of γ. From Figure 9, one can see the interesting observation of the position shift of the dominant energy minima from *between* the rows (at low values of φ_1) to *within* the rows (at high values of φ_1). This shift implies that the likelihood of forming horizontal (x-direction) C_{60} nanowires on pentacene is more likely at extreme values for φ_1 (e.g. 10° or 90°) where there would be a clear preference for C_{60} to be located between a row or within a row. For intermediate

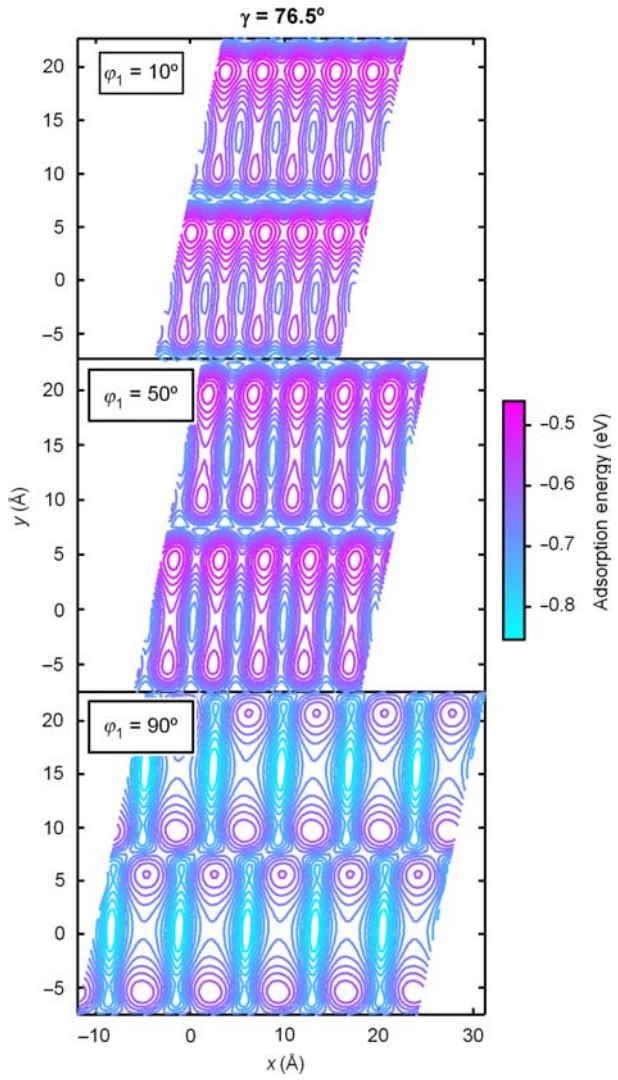

Figure 9. Contour adsorption energy plots of variably angled pentacene, at $\varphi_1 = 10°$, 50° and 90°, for the $\gamma = 76.5°$ case, with the key as in Figure 4. A stretch occurs in the *x*-direction for higher values of φ_1 in order to physically accommodate the pentacene molecules.

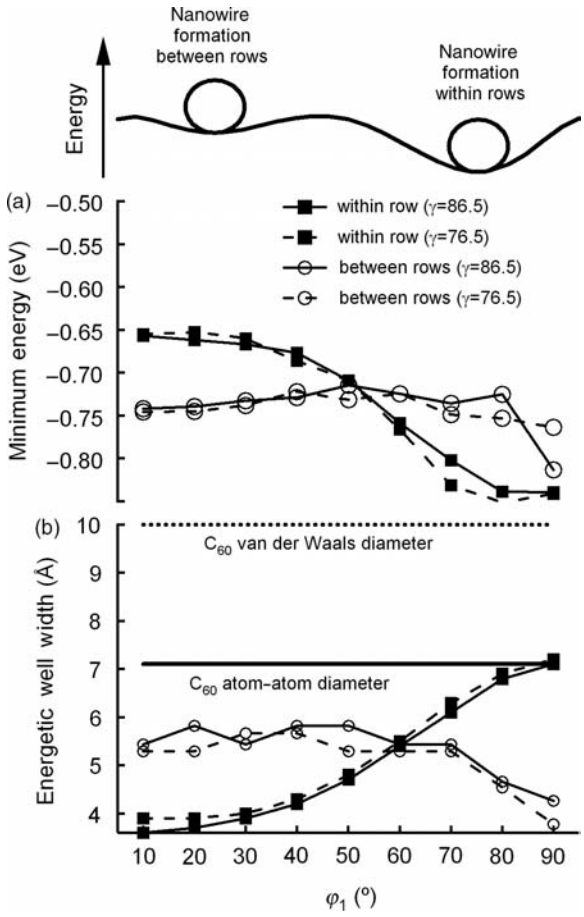

Figure 10. (a) Minimum energy and (b) width of the energy wells extracted from adsorption energy maps as a function of angle φ_1. Solid lines correspond to the $\gamma = 86.5°$ case; dashed lines to $\gamma = 76.5°$; filled squares correspond to energy wells between molecules within the pentacene rows, open circles correspond to those between the pentacene rows. The schematic diagram above both (a) and (b) illustrates the concept that higher values of φ_1 could be expected to yield more stable C_{60} nanowires.

values of φ_1, there is no such clear preference for horizontal C_{60} nanowires.

Figure 10(a) and (b) shows data taken from the surface energy plots that allow one to see more clearly where the dominant minimum energy transition occurs. Figure 10(a) shows the values of the energy minima both within and between the rows as we vary the angle made by the pentacene with the underlying substrate. The energy minimum transitions from being *between* pentacene rows to *within* the pentacene rows are at an angle of about $\varphi_1 = 50°$.

In addition to the *depth* of the energy wells, the *width* of the wells is also very important for determining the likelihood of C_{60} to reside in a particular site. If the C_{60} molecule cannot fit in a potential energy well, it is unlikely to reside there no matter how deep the well is. The wells occurring within the rows are ellipsoidal in shape, but the length in the *x*-direction (from saddle point to saddle point) was chosen to represent the 'width' of the well because it is the limiting dimension. The width of wells between rows was taken to be the width of the valley, specifically the maximum-to-maximum distance in the *y*-direction across the valley. Figure 10(b) shows the trend of these widths with the angle adopted by the pentacene (or its degree of flatness to the surface). At $\varphi_1 = 60°$, a transition occurs from a dominating between-row well width at low φ_1 values to a dominating within-row well width at high φ_1 values. This result corresponds approximately to the same transition shown in Figure 10(a); thus, the wider the energy well, the lower its energy.

We can ascertain the ability of a well to 'swallow' a C_{60} molecule into the surface by comparing the well widths on the pentacene surface to the diameter of C_{60} molecules; horizontal lines are shown in Figure 10(b) for the atom–atom and van der Waals diameters. Although both of these diameters are greater than any of the well widths obtainable by varying the angle that the Pn molecule adopts on the surface, clearly the greater the width of the well, the more likely a C_{60} molecule will reside there. For nanowires to form, it is probably unnecessary for the surface to engulf the C_{60} molecule; it only needs to 'cradle' it sufficiently well to be structure-directing. Summarising the results for the energy wells *between rows*: they are lower in energy and wider in width at low values of φ_1 (with the width reaching about 80% of the C_{60} atom–atom diameter and 55% of the van der Waals diameter) compared to high values of φ_1. The energy wells *within rows* are lower in energy and wider in width at high values of φ_1 (with the width reaching roughly 100% of the atom–atom diameter and 70% of the van der Waals diameter) as compared to low values of φ_1.

It is also important to compare these predictions to the experimental results of Dougherty et al., who found nanowires forming for a system characterised by a φ_1 angle of about 60°. Although it is difficult to tell if Dougherty et al.'s scanning tunnelling microscope (STM) images show nanowires occurring within or between rows, our results would predict that, at $\varphi_1 = 60°$, nanowire production would be more viable for C_{60} molecules located *within* Pn rows as judged more by the favourable energy and less by the width of the wells.

If one considers the *lowest overall* energy in Figure 10(a), the most stable configuration for the C_{60} occurs within a row of the flattest pentacene configuration, at φ_1 around 90° (as illustrated in the schematic energy diagram 'cartoon' in Figure 10). However, the extreme $\varphi_1 = 90°$ configuration appears unlikely because it minimises overlap with the neighbouring pentacene molecules' π-orbitals. At very low values of φ_1, we predict that metastable configurations of C_{60} might exist between the rows. Although one may not be able to control where the C_{60} ends up on the surface at thermal deposition conditions, these results suggest that by altering the short-axis tilt angle (long axis flat) of the bottom pentacene layer, which is achieved in experiments by choosing an appropriate substrate (e.g. varying the work function of the substrate metal), one could create a surface that encourages oriented growth of C_{60} nanowires.

5. Conclusions

In this paper, we have quantified the ability of the angular orientation of pentacene within a film to alter the diffusional and nanoscale adsorption properties of C_{60} through a computational study of Pn polymorphs. We have shown that C_{60} diffusion coefficients on thin film phase pentacene are approximately twice as high as that on bulk phase pentacene for experimentally realisable temperatures (200–400 K). This implies that C_{60} might have better growth properties on thin film phase pentacene because a higher diffusion coefficient generally leads to a greater tendency to wet the substrate and grow in an ordered fashion. The reasons for the lower diffusion coefficient of C_{60} on bulk phase pentacene were shown to be due to energy traps on the surface. In addition, C_{60} growth on bulk phase pentacene is probably less desirable because of its tendency for anisotropic diffusion, which could lead to unpredictable island shapes.

In our studies to emulate pentacene adsorbed on metal substrates, in which we varied the angle, φ_1, adopted by the short axis of the Pn molecules from 10° to 90°, we have used information about the width and depth of the adsorption energy wells to suggest whether nanowire formation is likely to occur. Low-energy sites on the adsorption energy surfaces switch from being located between the pentacene rows (short axis normal to the surface) to within the pentacene rows (short axis flat against the surface) as φ_1 increases. We suggest that this indicates a predilection for C_{60} nanowire production to be influenced by the angle adopted by the pentacene layers. We predict a more stable energy minimum within the Pn rows incorporating wells that are wide enough to cradle C_{60} molecules in such a way as to promote nanowire formation and occurring at a tilt angle of about 50°–60°, in good agreement with Dougherty's experiments. If Dougherty et al.'s STM images indeed show nanowires adsorbed *within* the Pn rows, their results – the only existing experimental evidence of C_{60} nanowire formation on pentacene – are fully consistent with ours. However, we also predict that less energetically stable nanowires could also be formed at a different orientation, i.e. between Pn rows, at low values of φ_1. Further experimental evidence to confirm these predictions would help complete this picture.

Acknowledgements

The authors acknowledge funding from the National Science Foundation through an IGERT Fellowship for RAC and for MRSEC funds administered by Cornell's Center for Materials Research (CCMR). The authors also thank D. Dougherty and B. Conrad for their useful discussions.

References

[1] O.D. Jurchescu, J. Baas, and T.T.M. Palstra, *Effect of impurities on the mobility of single crystal pentacene*, Appl. Phys. Lett. 84 (2004), pp. 3061–3063.

[2] V. Podzorov, V.M. Pudalov, and M.E. Gershenson, *Field-effect transistors on rubrene single crystals with parylene gate insulator*, Appl. Phys. Lett. 82 (2003), pp. 1739–1741.

[3] J.N. Haddock, X. Zhang, B. Domercq, and B. Kippelen, *Fullerene based n-type organic thin-film transistors*, Org. Electron. 6 (2005), pp. 182–187.

[4] S.J. Kang, Y. Yi, C.Y. Kim, S.W. Cho, M. Noh, K. Jeong, and C.N. Whang, *Energy level diagrams of C_{60}/pentacene/Au and pentacene/C_{60}/Au*, Synth. Met. 156 (2006), pp. 32–37.
[5] S.D. Wang, K. Kanai, Y. Ouchi, and K. Seki, *Bottom contact ambipolar organic thin film transistor and organic inverter based on C_{60}/pentacene heterostructure*, Org. Electron. 7 (2006), pp. 457–464.
[6] A.C. Mayer, M.T. Lloyd, D.J. Herman, T.G. Kasen, and G.G. Malliaras, *Postfabrication annealing of pentacene-based photovoltaic cells*, Appl. Phys. Lett. 85 (2004), pp. 6272–6274.
[7] S. Yoo, W.J. Potscavage, Jr, B. Domercq, S.-H. Han, T.-D. Li, S.C. Jones, R. Szoszkiewicz, D. Levi, E. Riedo, S.R. Marder, and B. Kippelen, *Analysis of improved photovoltaic properties of pentacene/C_{60} organic solar cells: Effects of exciton blocking layer thickness and thermal annealing*, Solid State Electron. 51 (2007), pp. 1367–1375.
[8] T. Minakata, H. Imai, M. Ozaki, and K. Saco, *Structural studies on highly ordered and highly conductive thin films of pentacene*, J. Appl. Phys. 72 (1992), pp. 5220–5225.
[9] D. Knipp, R.A. Street, A. Völkel, and J. Ho, *Pentacene thin film transistors on inorganic dielectrics: Morphology, structural properties, and electronic transport*, J. Appl. Phys. 93 (2003), pp. 347–355.
[10] L. Casalis, M.F. Danisman, B. Nickel, G. Bracco, T. Toccoli, S. Iannotta, and G. Scoles, *Hyperthermal molecular beam deposition of highly ordered organic thin films*, Phys. Rev. Lett. 90 (2003), 206101–206104.
[11] B.R. Conrad, J. Tosado, G. Dutton, D.B. Dougherty, W. Jin, T. Bonnen, A. Schuldenfrei, W.G. Cullen, E.D. Williams, J.E. Reutt-Robey, and S.W. Robey, *C_{60} cluster formation at interfaces with pentacene thin-film phases*, Appl. Phys. Lett. 95 (2009), 213302–213304.
[12] M. Satta, S. Iacobucci, and R. Larciprete, *Molecular adsorption and multilayer growth of pentacene on Cu(100): Layer structure and energetics*, Phys. Rev. B 75 (2007), 155401-1–155401-11.
[13] Y.L. Wang, W. Ji, D.X. Shi, S.X. Du, C. Seidel, Y.G. Ma, H.-J. Gao, L.F. Chi, and H. Fuchs, *Structural evolution of pentacene on a Ag(110) surface*, Phys. Rev. B 69 (2004), 075408–075412.
[14] H. Yamane, D. Yoshimura, E. Kawabe, R. Sumii, K. Kanai, Y. Ouchi, N. Ueno, and K. Seki, *Electronic structure at highly ordered organic/metal interfaces: Pentacene on Cu(110)*, Phys. Rev. B 76 (2007), pp. 165436–165445.
[15] J.H. Kang and X.-Y. Zhu, *Pi-stacked pentacene thin films grown on Au(111)*, Appl. Phys. Lett. 82 (2003), pp. 3248–3250.
[16] D. Choudhary, P. Clancy, and D.R. Bowler, *Adsorption of pentacene on a silicon surface*, Surf. Sci. 578 (2005), pp. 20–26.
[17] K.P. Weidkamp, C.A. Hacker, M.P. Schwartz, X. Cao, R.M. Tromp, and R.J. Hamers, *Interfacial chemistry of pentacene on clean and chemically modified silicon (001) surfaces*, J. Phys. Chem. B 107 (2003), pp. 11142–11148.
[18] Y. Zheng, S.K. Pregler, J.D. Myers, J. Ouyang, S.B. Sinnott, and J. Xue, *Computational and experimental studies of phase separation in pentacene: C_{60} mixtures*, J. Vac. Sci. Technol. B 27 (2009), pp. 169–179.
[19] I. Salzmann, S. Duhm, R. Opitz, R.L. Johnson, J.P. Rabe, and N. Koch, *Structural and electronic properties of pentacene–fullerene heterojunctions*, J. Appl. Phys. 104 (2008), pp. 114518–114528.
[20] Y. Yi, V. Coropceanu, and J.-L. Brédas, *Exciton-dissociation and charge-recombination processes in pentacene/C_{60} solar cells: Theoretical insight into the impact of interface geometry*, J. Am. Chem. Soc. 131 (2009), pp. 15777–15783.
[21] S.D. Ahn, S.Y. Kang, Y.E. Lee, M.J. Joung, C.A. Kim, and K.S. Suh, *Flexible Electronics – Materials and Device Technology*, Spring Meeting of the Materials Research Society, San Francisco, CA, 2003.
[22] I.P.M. Bouchoms, W.A. Schoonveld, J. Vrijmoeth, and T.M. Klapwijk, *Morphology identification of the thin film phases of vacuum evaporated pentacene on SiO_2 substrates*, Synth. Met. 104 (1999), pp. 175–178.
[23] T. Kakudate, N. Yoshimoto, and Y. Saito, *In-plane Structure and Polymorphism of Pentacene Thin Films, Organic Electronics – Materials, Devices and Applications*, Fall Meeting of the Materials Research Society, Boston, MA, 2006.
[24] J. Goose, P. Clancy, and M. Thompson, *Direct melt processing of pentacene at temperatures above 1000°C by pulsed laser irradiation*, Appl. Phys. Lett. 93 (2008), pp. 183306-1–183306-3.
[25] J.E. Northrup, M.L. Tiago, and S.G. Louie, *Surface energetics and growth of pentacene*, Phys. Rev. B 66 (2002), pp. 121404–121407.
[26] R.B. Campbell, J.M. Robertson, and J. Trotter, *The crystal structure of hexacene, and a revision of the crystallographic data for tetracene and pentacene*, Acta Cryst. 15 (1962), pp. 289–290.
[27] H. Yoshida, K. Inaba, and N. Sato, *X-ray diffraction reciprocal space mapping study of the thin film phase of pentacene*, Appl. Phys. Lett. 90 (2007), pp. 181930–181932.
[28] K. Itaka, M. Yamashiro, J. Yamaguchi, M. Haemori, S. Yaginuma, Y. Matsumoto, M. Kondo, and H. Koinuma, *High-mobility C_{60} field-effect transistors fabricated on molecular-wetting controlled substrates*, Adv. Mater. 18 (2006), pp. 1713–1716.
[29] R. Cantrell and P. Clancy, *A computational study of surface diffusion of C_{60} on pentacene*, Surf. Sci. 602 (2008), pp. 3499–3505.
[30] D.B. Dougherty, W. Jin, W.G. Cullen, G. Dutton, J.E. Reutt-Robey, and S.W. Robey, *Local transport gap in C_{60} nanochains on a pentacene template*, Phys. Rev. B 77 (2008), pp. 073414–073417.
[31] *TINKER: Software Tools for Molecular Design*, 2009; software available at http://dasher.wustl.edu/tinker/.
[32] E. Kuwahara, Y. Kubozono, T. Hosokawa, T. Nagano, K. Masunari, and A. Fujiwara, *Fabrication of ambipolar field-effect transistor device with heterostructure of C_{60} and pentacene*, Appl. Phys. Lett. 85 (2004), pp. 4765–4767.
[33] N.L. Allinger, Y.H. Yuh, and J.H. Lii, *Molecular mechanics. The MM3 force field for hydrocarbons. 1*, J. Am. Chem. Soc. 111 (1989), pp. 8551–8566.
[34] J.E. Goose and P. Clancy, *Exploring the energetic deposition of pentacene on pentacene through molecular dynamics simulations*, J. Phys. Chem. C 111 (2007), pp. 15653–15659.
[35] J.M. Pacheco and J.P. Prates Ramalho, *First-principles determination of the dispersion interaction between fullerenes and their intermolecular potential*, Phys. Rev. Lett. 79 (1997), pp. 3873–3876.
[36] K.S. Fa and E.K. Lenzi, *Power law diffusion coefficient and anomalous diffusion: Analysis of solutions and first passage time*, Phys. Rev. E 67 (2003), pp. 061105–061111.

Appendix

In studies where we vary the short-axis angle of the pentacene molecules with the substrate, it is important to obtain the most realistic pentacene surface that a C_{60} molecule is likely to encounter, given that we do not know the characteristic unit cell parameters for all these hypothetical situations. To address the lack of unit cell parameters, we have devised a procedure described below and summarised as a flow chart in Figure A1, which involves a series of potential energy minimisations using MM3, as a means to provide realistic tilted pentacene structures.

In this appendix, we describe a 'flat' pentacene unit cell as having two pentacene molecules: one, denoted with the number 1 as Pn_1, lies on the bottom directly above some unspecified substrate material. The other, denoted with the number 2 as Pn_2, lies on top and slightly askew of Pn_1 making a total of two pentacene layers per unit cell (see Figure 2). The unit cell parameters found from the procedure described in Figure A1 are summarised in Table 1. Since Pn_1 and Pn_2 comprise a one unit cell thick layer, the unit cell parameters c, α and β are irrelevant. The independent variable is the angle φ_1 made by Pn_1's short axis with the surface normal (see Figure 2(b)), assuming that Pn_1's long axis is parallel to the substrate. The lattice parameter, a, depends on the value chosen for φ_1, with larger a values corresponding to larger φ_1 values. The lattice parameters, b and γ, which are assumed not to vary with φ_1, were obtained by MD snapshots similar to the one shown in Figure A2. The angles θ_1 and θ_2 are the anticlockwise angles that the long axes of Pn_1 and Pn_2, respectively, make with the b unit cell vector (see Figure 2(a)).

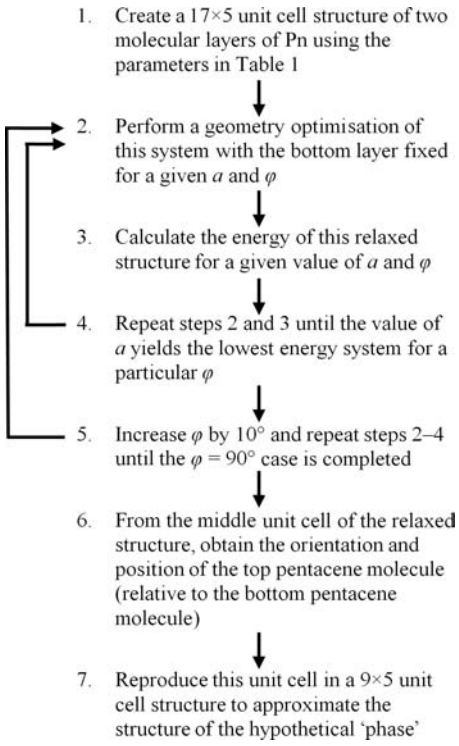

Figure A1. Schematic diagram of the process used to determine the approximate structure for variably angled pentacene polymorphs.

The θ_2 values were also extracted from MD snapshots, and we assumed that $\theta_1 = \theta_2$ initially.

An MD simulation of pentacene on a silicon substrate (see snapshot in Figure A2) was used to obtain the parameters b, γ and θ_2 described above. Although MM3 potential parameters for silicon have not been optimised for this system, we knew from our earlier work that it was sufficiently realistic to cause the pentacene to lie face down on the substrate, the only necessary prerequisite. The MD simulation was performed with 48 pentacene molecules on a Si(001) surface, which was three atomic layers thick. Periodic boundary conditions were applied in the x- and y-directions to allow the face-down pentacene cluster to move freely. The simulation was thermalised at 300 K in the constant-temperature NVT ensemble for 50 ps and then run in the NVE ensemble for 2 ns.

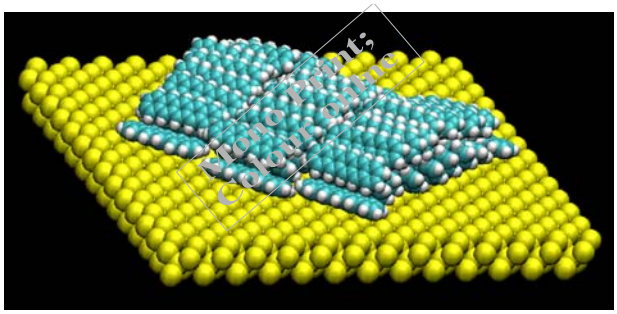

Figure A2. MD snapshot of two layers of 24 pentacene molecules (48 total molecules) on three atomic layers of a Si(001) surface. Aqua-coloured carbon atoms and white hydrogen atoms make up the pentacene molecules; yellow-coloured silicon atoms make up the Si(001) surface (colour online).

Taking five different snapshots, each 300 ps apart, we extracted values for b and γ (excluding the molecules on the edges) by calculating the centre-to-centre distances of the top layer pentacene molecules. For both b and γ, there were 10 values to extract in each snapshot, making a total of 50 values of b and γ. These values are shown as histograms in Figure A3(a) and (b). As illustrated in Figure A3(a) and (b), the average value for the lattice parameter b is 15.6 Å and that for γ is 86.5°. The distribution for γ is skewed in the positive direction, so the most probable value is less than the exact average value. We speculate that this is due to our capturing some shearing event of the unit cell rows with respect to one another.

In this paper, we also consider the case where $\gamma = 76.5°$, to see the effect of a 10° change in γ on the energy properties of the surface. This change represents our uncertainty in γ and allows us to gauge the sensitivity of the results to our choice of γ. The values for θ_2 were also extracted from these snapshots, but, in this case, both the edge molecules and the top and bottom row molecules were excluded to ignore any edge effects. There were five values of θ_2 to extract in each snapshot, making a total of

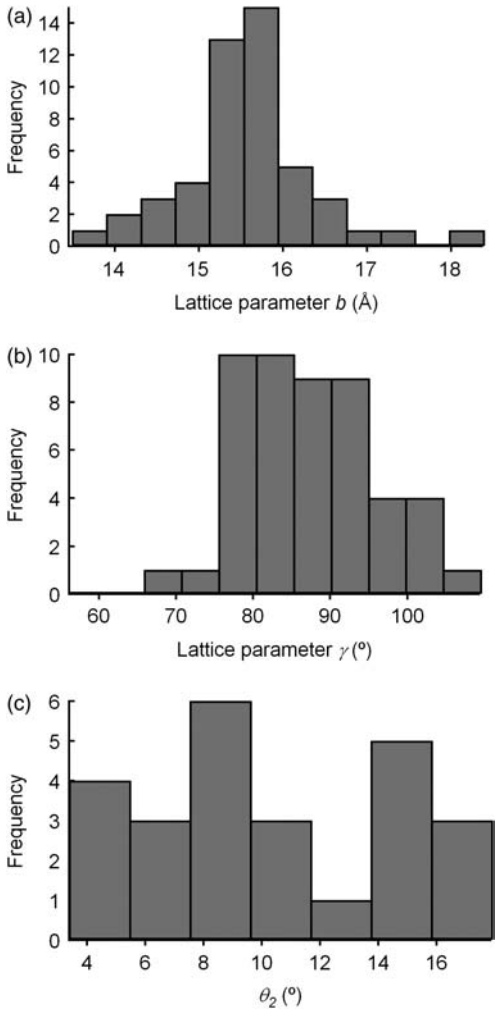

Figure A3. Histograms of extracted values of parameters (a) b, (b) γ and (c) θ_2 from five MD snapshots. Histograms of b and γ are based on 50 values, that for θ_2 is based on 25 values.

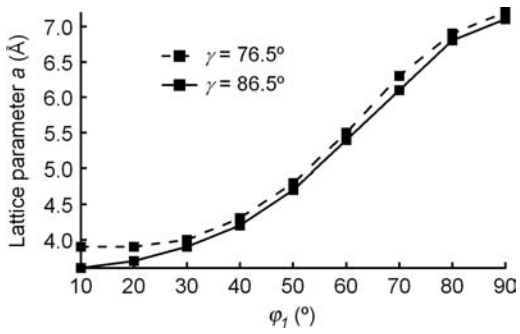

Figure A4. Lattice parameter, a, as a function of φ_1, the degree of 'flatness' of the pentacene molecules on the substrate for both $\gamma = 76.5°$ (dashed line) and $\gamma = 86.5°$ (solid line).

25 values of θ_2. These values are shown as a histogram in Figure A3(c). The distribution of θ_2 values appears to be reasonably uniform, with an average value of 10.1°.

Once the values for b, γ and θ_2 were obtained from the MD snapshots, we could begin to create a 17×5 unit cell layer of the flat pentacene without a substrate. As an initial configuration, we assume that $\theta_1 = \theta_2$, $\varphi_1 = \varphi_2$ and that the distance vector between Pn_1 and Pn_2, denoted as $\mathbf{d}_{12}$, is $\langle \frac{1}{2}a, 0, 5\ \text{Å} \rangle$. The next step is to determine appropriate values for a based on a given value of φ_1. We varied φ_1 from 10° to 90°, in increments of 10°, and for each value of φ_1, different values of a were tested. For each a–φ_1 combination tested, we fixed the bottom pentacene layer and allowed the top pentacene layer to relax in a geometry minimisation. For a particular value of φ_1, we choose the value of a (to within a tenth of an angstrom) for which the geometry-minimised structure had the lowest energy; the other non-minimising a values are not considered. The values of a that gave minimum energy configurations for different values of φ_1 are shown in Figure A4 for two cases of $\gamma = 76.5°$ and 86.5°. There is no significant difference between the lattice parameter a values for $\gamma = 76.5°$ and 86.5°, but each a–γ–φ_1 combination, as shown in Figure A4, is treated as a unique system for subsequent calculations.

At this point, it is beneficial to double-check some of the values obtained so far against those in the literature. Kang et al. [15] grew two layers of pentacene lying flat on Au(111) at room temperature and found a, b and γ values of 5.7 Å, 15.5 Å and 84°, respectively, through high-resolution STM imaging. Dougherty et al. [30] grew two layers of pentacene lying flat on Ag(111) at room temperature and calculated b to be 16 Å through high-resolution STM imaging; values for a and γ were not given. Even though Kang et al. used a gold substrate and Dougherty et al. used

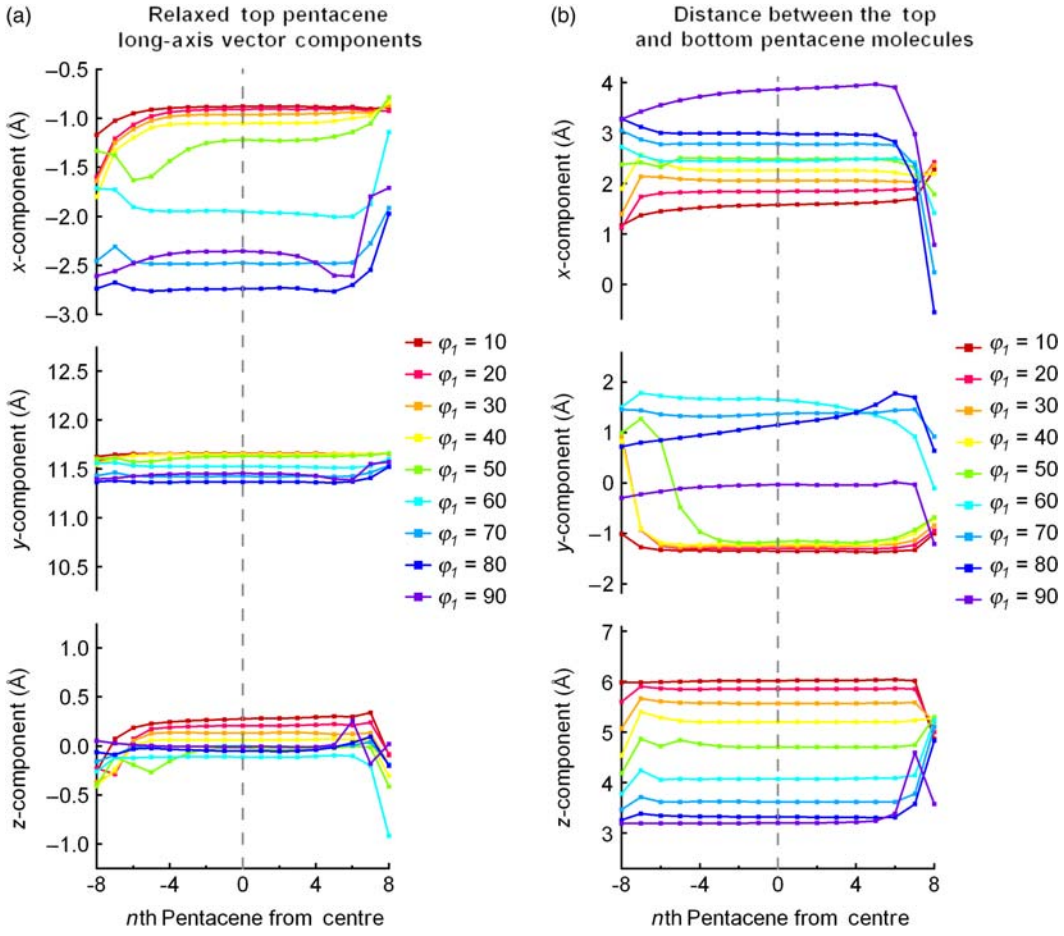

Figure A5. Convergence of the middle row of 17×5 pentacene molecules in the geometry-minimised variably angled pentacene structures. The convergence is measured by (a) the vector components of the top pentacene molecule in each unit cell and (b) the distance between the top and bottom pentacene molecules in each unit cell.

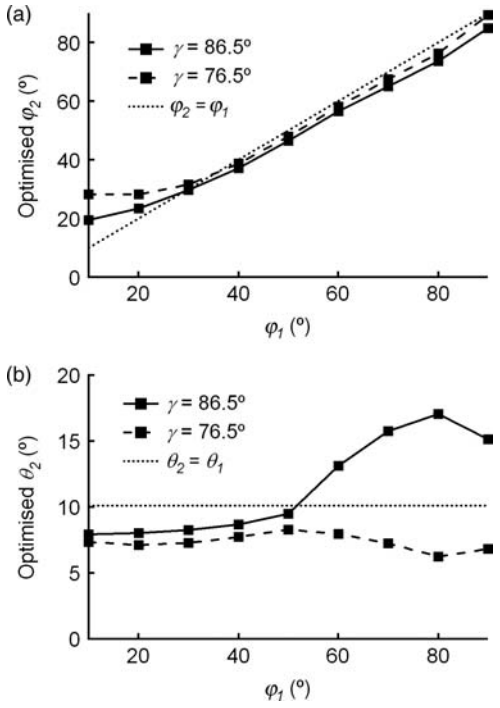

Figure A6. For each φ_1, deviations of the (a) optimised φ_2 and (b) optimised θ_2 via geometry optimisation as compared to their initial values, φ_1 and θ_1, respectively.

a silver one, their values for b match quite nicely with one another and importantly, match our calculations with a value of $b = 15.6$ Å. Kang et al.'s values for a and γ also match up quite well with the values that we found ($a = \sim 4-7$ and $\gamma = 85.6°$) through MD simulation and energy minimisations.

To create a 'flat' pentacene surface for the adsorption energy calculations, we extract the middle unit cell from the geometry-minimised 17×5 unit cell structure for each γ–φ_1 combination as the exemplar for the system. But to make sure that the 17×5 unit cell structures were large enough that the middle unit cell has a converged structure, we calculated the vector components of the long axis for the top pentacene molecules for all of the top pentacene molecules in the middle row (see Figure A5(a)). We also checked the $\mathbf{d}_{12}$ vector components to make sure that they converged (see Figure A5(b)). Unlike in most convergence graphs, the convergence seen in Figure A5 occurs towards the centre ($x = 0$, where x refers to the nth pentacene in the middle row). Each top pentacene molecule in the middle row of the 17×5 structure corresponds to one of the 17 points on the x-axis. Thus, according to Figure A5, the overall structure of the middle unit cell does indeed converge towards the centre.

In addition to determining the sufficiency of convergence of the structure of the middle unit cell, it is important to point out how much φ_2 and θ_2 changed from their initial values, set equal to φ_1 and θ_1, respectively. As shown in Figure A6(a), for the φ_2 values, there is only significant divergence from the initial value at low φ_1 values. Low φ_1 values also correspond to low lattice parameter a values. Low values of a correspond to a more compact unit cell, explaining why φ_2 values are higher at lower φ_1. As shown in Figure A6(b) for θ_2 values, there is only significant divergence from the initial value at higher φ_1 values, especially for the $\gamma = 86.5°$ case.

After achieving sufficient convergence of the structure of the middle unit cell in each case, as shown in Figure A5, we repeated these unit cells in a 9×5 array for each γ–φ_1 combination. We choose a 9×5 array because it is large enough to avoid any edge effects of the adsorption energy calculations and it is small enough that the calculations do not take too long. These 9×5 arrays for each γ–φ_1 combination are the structures used for the C_{60} surface adsorption energy calculations shown in Figure 9.